The published paper may be found at: https://asmedigitalcollection.asme.org/GT/proceedings-abstract/GT2022/86007/V03BT04A021/1148780
For citation:
Kutkan, H, Amato, A, Campa, G, Tay-Wo-Chong, L, & Æsøy, E. "LES of Turbulent Premixed CH_4/H_2/Air Flames With Stretch and Heat Loss for Flame Characteristics and Dynamics." *Proceedings of the ASME Turbo Expo 2022: Turbomachinery Technical Conference and Exposition. Volume 3B: Combustion, Fuels, and Emissions*. Rotterdam, Netherlands. June 13–17, 2022. V03BT04A021. ASME. https://doi.org/10.1115/GT2022-82397

LES OF TURBULENT PREMIXED CH_4/H_2/AIR FLAMES WITH STRETCH AND HEAT LOSS FOR FLAME CHARACTERISTICS AND DYNAMICS

Halit Kutkan[1,2], Alberto Amato[1], Giovanni Campa[1], Luis Tay-Wo-Chong[3], Eirik Æsøy[4]

[1]Ansaldo Energia S.p.A., Genoa, Italy
[2]Universita degli study di Genova, Genoa, Italy
[3]Ansaldo Energia Switzerland AG, Baden, Switzerland
[4]Norwegian University of Science and Technology, Trondheim, Norway

ABSTRACT

This paper presents large eddy simulation (LES) turbulent combustion models for premixed methane/hydrogen/air mixtures which account for stretch, heat loss and Lewis number effects by means of a previously proposed turbulent flame speed expression [1]. *In this expression stretch and heat loss effects are introduced by means of strained non-adiabatic laminar consumption speed calculations in fresh-to-burnt counter flow configurations with detailed chemistry, and preferential diffusion of hydrogen is accounted for by calculating an effective Lewis number of the reactants.*

To validate and analyze the performance of the models, large eddy simulations of fully premixed atmospheric bluff body stabilized methane/hydrogen/air flames are compared against experimental measurements [2, 3]. *Heat release distributions and mean flame shapes are compared against OH^* chemiluminescence data. Flame dynamics are investigated by extracting flame transfer functions (FTFs) with system identification (SI) methods and comparing them with measured FTFs from experiments.*

Keywords: LES combustion modelling, CH_4/H_2/air premixed flames, flame dynamics, stretch and heat losses.

NOMENCLATURE

Subscripts

u	Unburnt mixture (i.e. reactants)
p	Burnt mixture (i.e. products)
SGS	Sub-grid-scale property
t	Turbulent property

Superscripts

$\overline{\ }$	Reynolds averaged/filtered
$\sim$	Favre averaged/filtered

Greek letters

α	Thermal diffusivity
β	Heat loss coefficient
Σ	Flame surface density
Δ_{LES}	LES filter length
Γ_K	Efficiency function
δ_{L0}	Laminar flame thickness
δ_t	Turbulent flame brush thickness
ε	Turbulence dissipation rate
κ	Flame stretch
ν	Kinematic viscosity
$\dot{q}$	Total heat release rate per volume
ρ	Density
Φ	Equivalence ratio
$\dot{\omega}$	Reaction rate

Latin letters

c	Progress variable (0 in the reactants, 1 in the products)
h	Enthalpy
k	Turbulence kinetic energy
l	Turbulent length scale
u	Velocity
x	Volumetric (or molar) fraction

Other

FTF	Flame transfer function
HTC	Heat transfer coefficient
SI	System identification
ΔH_c^o	Lower heating value
Le^*	Effective Lewis number
S_c	Laminar flame consumption speed
Sc_t	Turbulent Schmidt number
S_{L0}	Laminar unstretched adiabatic flame speed
S_t	Turbulent flame speed

1. INTRODUCTION

Recent international commitments towards carbon neutral energy production are motivating an increased interest in the development of gas turbine engines able to operate with hydrogen blended fuels. However, current lean-premixed

*Corresponding author: halit.kutkan@edu.unige.it

combustor technologies are not yet able to handle reliably the full range of 0-100% hydrogen contents blended with natural gas. One challenge is to predict the flame stabilization and dynamics when hydrogen, which has a higher reactivity than natural gas, is added to the fuel. In lean-premixed combustors, flames are stabilized by recirculating hot gases with the help of bluff-bodies and/or swirlers. Depending on the interplay between hydrogen addition, heat losses and flame stretch in the hot gas recirculation zones, different flame stabilization shapes (such as M-flames, V-flames or detached flames) can be present in a combustor. Modelling of such stabilization shapes are crucial for the prediction of the combustor dynamics response [2–4]. Several efforts have been made in the literature to model the effects of stretch, heat loss and preferential diffusion of hydrogen.

Mercier et al. [5] investigated the impact of heat losses in LES context with the FTACLES (Filtered Tabulated Chemistry for LES) combustion modelling approach for 60% and 90% vol. H_2 in fuel for CH_4/H_2/air premixed swirl flames and concluded that the inclusion of heat losses produced flame stabilization in agreement with experiments. However, it was pointed out that the model could be improved by explicitly modelling the effect of flame stretching. Chatelier et al. [6] used the same approach and burner configuration for 60% vol. H_2 content in fuel for CH_4/H_2/air premixed flame to extract FTFs. Despite reasonably well predicted mean flame shape and FTF, excluding explicit modelling of flame stretch caused over-predicted heat release rates at the outer shear layer. Tay-Wo-Chong et al. [7] proposed a LES version of the ExtTFC (Extended Turbulent Flame Closure) model which accounts for stretch and heat loss effects in CH_4/air flames and showed that the inclusion of stretch and heat loss effects are required to predict flame stabilization and dynamics correctly. A similar approach has later been used by Nassini et al. [8] for industrial burner simulations. Recently, Kutkan et al. showed in RANS (Reynolds averaged Navier Stokes) context [1, 9] that the inclusion of Lewis number effects together with stretch and heat loss effects into algebraic combustion models has a good potential to model CH_4/H_2/air flame shapes and stabilization. The objective of the present work is to extend the previously proposed modelling approaches [1, 9] to large eddy simulations (LES).

The rest of the paper is organized as follows: Section 2 describes the LES combustion modelling approaches based on the proposed turbulent flame speed expression which includes stretch and heat loss modelling. Two different reaction rate closure models (described in section 2.1 and section 2.2) are compared in this paper. The experimental setup and numerical methods are illustrated in section 3. Cold flow, unforced and forced reacting flow results in comparison with experiments are presented and commented in section 4. Finally, in section 5 the main conclusions of the present study are summarized.

2. LES MODELLING OF TURBULENT PREMIXED COMBUSTION

Turbulent premixed combustion can be modelled by solving a Favre averaged/filtered combustion progress variable $\tilde{c}$ transport equation [10, 11].

$$\frac{\partial(\bar{\rho}\tilde{c})}{\partial t}+\frac{\partial\left(\bar{\rho}\tilde{u}_j\tilde{c}\right)}{\partial x_j}+\frac{\partial}{\partial x_j}\left(\bar{\rho}\widetilde{u_j c}-\bar{\rho}\tilde{u}_j\tilde{c}\right)=\frac{\partial}{\partial x_j}\left(\overline{\rho D\frac{\partial c}{\partial x_j}}\right)+\bar{\dot{\omega}} \quad (1)$$

Where $\bar{}$ and $\tilde{}$ refer to filtered and Favre filtered quantities. Modelling the unresolved scalar fluxes from standard gradient assumption and following [12] to model the right hand side (RHS) from flamelet approach, Eq. (1) reduces to [10]:

$$\frac{\partial(\bar{\rho}\tilde{c})}{\partial t}+\frac{\partial\left(\bar{\rho}\tilde{u}_j\tilde{c}\right)}{\partial x_j}=\frac{\partial}{\partial x_j}\left(\bar{\rho}\frac{\nu_{SGS}}{Sc_t}\frac{\partial\tilde{c}}{\partial x_j}\right)+\rho_u\langle S_c\rangle_s\Sigma \quad (2)$$

where ν_{SGS} represents the sub-grid-scale turbulent viscosity, $Sc_t=0.7$ is the turbulent Schmidt number, ρ_u is the unburnt gas density, $\langle S_c\rangle_s$ is the flame surface averaged laminar consumption speed and Σ is the sub-grid-scale flame surface density, which needs to be modelled in the LES framework.

2.1 Extended turbulent flame speed closure model for CH_4/H_2/air mixtures in LES context (ExtH_2TFC)

The turbulent flame closure (TFC) combustion model assumes that the reaction rate source term can be expressed as [13]:

$$\bar{\dot{\omega}}=\rho_u\langle S_c\rangle_s\Sigma=\rho_u S_{t,SGS}|\nabla\tilde{c}| \quad (3)$$

where $|\nabla\tilde{c}|$ is the modulus of the Favré-averaged progress variable gradient and $S_{t,SGS}$ is the sub-grid-scale turbulent flame speed, which is modeled as described in section 2.3.

2.2 Extended Lindstedt and Vaos model for CH_4/H_2/air mixtures in LES context (ExtH_2LV)

Lindstedt and Vaos derived the following RANS closure by assuming $\langle S_c\rangle\approx S_{L0}$, and modelling the flame surface density Σ from fractal theories [14].

$$\bar{\dot{\omega}}=C_R\rho_u\frac{S_{L0}}{u_{\eta_K}}\frac{\varepsilon}{k}\tilde{c}(1-\tilde{c}) \quad (4)$$

In Eq. (4), C_R is the reaction rate coefficient that needs to be tuned, $u_{\eta_K}=(\nu\varepsilon)^{0.25}$ is the Kolmogorov velocity scale, and k and ε are the turbulent kinetic energy and dissipation rate respectively. The following RANS closure was proposed in [9] by replacing $C_R S_{L0}$ with S_t, and the resulting model was entitled as the ExtH_2LV model.

$$\bar{\dot{\omega}}=\rho_u\frac{S_t}{u_{\eta_K}}\frac{\varepsilon}{k}\tilde{c}(1-\tilde{c}) \quad (5)$$

Further derivation of the ExtH$_2$LV model is provided in the Appendix A. Using relations given with Eq. (6) LES formulation for this model is derived in Eq. (7):

$$k \approx k_{SGS}, \qquad \varepsilon \approx \varepsilon_{SGS} \approx \frac{k_{SGS}^{1.5}}{\Delta_{LES}} \tag{6}$$

$$\bar{\dot{\omega}} = \rho_u \frac{S_{t,SGS}}{u_{\eta_{K,SGS}}} \frac{\sqrt{k_{sgs}}}{\Delta_{LES}} \tilde{c}(1-\tilde{c}) \tag{7}$$

where $u_{\eta_{K,SGS}} \approx (\nu \varepsilon_{SGS})^{0.25}$, k_{SGS}, $S_{t,SGS}$ are the sub-grid-scale Kolmogorov velocity, turbulent kinetic energy and turbulent flame speed, respectively, and Δ_{LES} is the LES filter length.

2.3 Turbulent flame speed for CH$_4$/H$_2$/air flames

The turbulent flame speed, used in this study was proposed in [1, 9] in the RANS context as:

$$S_t = S_c + \frac{0.4}{\sqrt{Le^*}} u'^{0.8} S_c^{0.45} \alpha_u^{-0.25} l_t^{0.25} \tag{8}$$

where S_c, Le^*, u', α_u and l_t are the laminar non-adiabatic stretched consumption speed, effective Lewis number, turbulent velocity, unburnt thermal diffusivity and turbulent length scale, respectively. Stretch and heat loss effects are included in the S_c as described in the next section. The effective Lewis number Le^* is calculated for CH$_4$/H$_2$/air mixtures as proposed in [15]:

$$Le^* = \frac{\alpha}{x_{H_2} D_{H_2} + x_{CH_4} D_{CH_4}} \tag{9}$$

where, x_{H_2} and x_{CH_4} are the mole fractions of species in the fuel, D_{H_2} and D_{CH_4} are the binary mass diffusion coefficients with respect to inert N_2 gas, and α is the thermal diffusivity of the mixture. All transport properties in Eq. (9) are evaluated at the temperature, corresponding to the maximum heat release rate in the 1D unstretched adiabatic laminar flame calculation [1, 9].

For LES implementation Eq. (8) is modified as:

$$S_{t,SGS} = S_c + \frac{A}{\sqrt{Le^*}} u'^{0.8}_{SGS} S_c^{0.45} \alpha_u^{-0.25} \Delta_{LES}^{0.25} \tag{10}$$

where the turbulent fluctuation velocity and turbulent length scale are modelled using the sub-grid-scale turbulent kinetic energy and the filter length as:

$$u' \approx u'_{SGS} = \sqrt{\frac{2}{3} k_{SGS}}, \; l_t \approx \Delta_{LES} = V_{cell}^{1/3} \tag{11}$$

with V_{cell} representing the computation cell volume.

In Eq. (10), the coefficient A for the ExtH$_2$LV model is equal to the one in RANS ($A = 0.4$), while for the ExtH$_2$TFC model, a coefficient readjustment to $A = 0.7$ was implemented. Coefficient readjustment was shown to be necessary in several studies [16–18] when adapting TFC models, based on progress variable gradient, from RANS to LES. The value $A = 0.7$ was adjusted based on a good agreement in the experimental mean flame length with the 0% H_2 case, as shown in section 4.2. The values of the coefficients in both LES models, were kept the same for all the mixtures listed in Table 1.

2.4 Stretch and heat loss modelling

Stretch and heat loss modelling is composed of two steps. In the first step, laminar flame consumption speeds S_c are tabulated for different levels of strain and heat loss. S_c values are calculated in a fresh-to-burnt counter flow flame configuration in Cantera 2.4.0 [19] using the detailed chemical mechanism Aramco-Mech 1.3 [20], and transport properties modelled with a multi-component transport formulation and Soret thermal diffusion. Different levels of heat loss β are simulated by decreasing the burnt mixture temperature T_p below the adiabatic flame temperature T_{ad} according to Eq. (12), while keeping the unburnt mixture temperature T_u constant. Flame stretch is evaluated from the maximum velocity gradient at the unburnt side (Eq. (12)) and raised by gradually increasing the flow velocities of burnt and unburnt jets.

$$\beta = \frac{T_p - T_u}{T_{ad} - T_u}, \quad \kappa = max\left|-\frac{\partial u}{\partial x}\right| \tag{12}$$

Laminar consumption speeds are calculated with Eq. (13) under varying strain κ and heat loss β conditions. Look-up tables are formed for the mixtures listed in Table 1.

$$S_c = \frac{1}{\rho_u \Delta H_c^o Y_f} \int_{-\infty}^{+\infty} \dot{q}\, dx \tag{13}$$

where ρ_u, ΔH_c^o, Y_f and $\dot{q}$ are the unburnt mixture density, lower heating value, mass fraction of the fuel, and total heat release rate per unit volume, respectively. Further detail on tabulation can be found in refs [1, 9].

The second step is the evaluation of stretch and heat losses in LES. Following [7], flame stretch κ can be evaluated in the LES framework by accounting for the resolved scales κ_{mean} and the sub-grid-scale κ_{SGS} contributions.

$$\kappa = \underbrace{\left(\delta_{ij} - \widetilde{n_i}\widetilde{n_j}\right)\frac{\partial \widetilde{u_i}}{\partial x_j}}_{\kappa_{mean}} + \underbrace{\Gamma_K\left(\frac{k_{SGS}}{S_{L0}}, \frac{\Delta_{LES}}{\delta_{L0}}\right)\frac{\sqrt{k_{sgs}}}{\Delta_{LES}}\left[\frac{1}{Le}(1.76 + \tanh(Le-2))\right]}_{\kappa_{SGS}} \tag{14}$$

In Eq. (14), δ_{ij} is the Kronecker delta and n_i is the component of local vector normal to the flamelet $\vec{n}$, which is modelled as [8]:

$$\vec{n} = \frac{\nabla \tilde{c}}{|\nabla \tilde{c}|} \tag{15}$$

The term Γ_K represents the efficiency function, whose evaluation is given in detail in [7]. δ_{L0} is the adiabatic unstretched thermal laminar flame thickness calculated from $\delta_{L0} = (T_{ad} - T_u)/\max(dT/dx)$ in a 1D unstretched flame. The term in brackets in Eq. (14), containing the Lewis number Le of the fuel was proposed in [21] to better fit average turbulent flame stretch values computed from direct numerical simulations of CH_4/H_2/air and C_3H_8/H_2/air flames. For $Le = 1$ this term is equal to 1 thus recovering the κ_{SGS} expression used in [7, 22, 23] for CH_4/air flames. For mixtures with hydrogen, Le is calculated from $Le = x_{CH_4}\,\alpha/D_{CH_4} + x_{H_2}\,\alpha/D_{H_2}$ as indicated in [21].

The heat loss parameter β is calculated in LES following [23]:

$$\beta = 1 - \frac{h_u - \tilde{h}}{\tilde{c} Y_f \Delta H_c^0} \qquad (16)$$

where h_u, Y_f and ΔH_c^0 are total unburnt enthalpy (sensible plus the standard formation enthalpy), fuel mixture fraction and lower heating value of the fuel, respectively. The local enthalpy $\tilde{h}$ is obtained by solving the Favre filtered enthalpy transport equation.

In summary, Eq. (14) and (16) are used for stretch and heat loss evaluation over the LES computational domain and based on their values, laminar consumption speed S_c is interpolated from the look-up tables, which were formed by means of Eq. (12) and (13).

3. EXPERIMENTAL AND NUMERICAL MODEL SETUP

3.1 Experimental setup

The experiments modeled in this paper were carried out in the atmospheric test rig described in [2]. As shown in Figure 1, the rig consists of a cylindrical combustion chamber with inner diameter of 44 mm, 3 mm thick quartz walls, and a length of 75 mm. The combustor has been operated with 5 different mixtures of CH_4/H_2/air premixed gas. The mixture properties and inlet conditions are presented in the Table 1. The reactants inlet temperature is equal to 296 K for all the cases.

TABLE 1. OPERATING CONDITIONS IN TERMS OF THERMAL POWER, VOLUME FRACTION OF H_2 IN THE FUEL, EQUIVALENCE RATIO AND INLET BULK VELOCITY

$P\ [kW]$	Vol_{H_2} [%]	Φ [-]	$u_{inlet}\ [m/s]$
7	0	0.7	11.8
7	25.2	0.7	11.8
7	56.6	0.7	11.5
7	67	0.7	11.4
7	100	0.4	17.1

Particle image velocimetry (PIV) measurements of the cold flow were carried out by ensemble averaging of 5000 vector fields. OH^* chemiluminescence imaging was captured using the same camera setup as for PIV and the planar view was obtained using a 3 point Abel deconvolution.

Acoustic forcing was provided by horn drivers with harmonic signal at a range of discrete frequencies [200-2200 Hz]. The flame response is measured by the spatially integrated heat release rate Q by tracking the measured radiation emitted from OH^* radicals, using a photo multiplier tube (PMT) equipped with a ultra-violet (UV) band pass filter. Since the flames are fully premixed, the PMT signal $I(t)$ is assumed to be proportional to the global heat release rate. Velocity fluctuations $\hat{u}'_{ref}(t)/\bar{\hat{u}}_{ref}$ at the dump plane ($z = 0\ mm$ in Figure 1) are computed with the multiple microphone method (MMM). Further details on the experimental setup and the measurement methods can be found in [2].

3.2 Numerical model setup

CFD simulations were performed in Ansys Fluent 2019 R3 [24] on the 360º 3D geometry. The combustion chamber computational domain has been doubled in length compared to the experimental setup to increase the distance between the outlet boundary condition and the flame in order to provide flow continuity. Figure 1 shows the geometry, dimensions, and boundary conditions of the computational domain. The inlet turbulence is calculated with a spectral synthesizer method having 5% turbulence intensity and 0.014 m of hydraulic diameter (same conditions of previous RANS in [1, 9]).

The mesh was created using the BetaCAE ANSA 20 software, having around 14 million cells in total and its section view is shown in Figure 2. The averaged y^+ value in the domain is around unity ($y^+ \approx 1$) having $y^+ \approx 1.5$ in the inlet pipe section and $y^+ \approx 0.7$ in the combustion chamber section.

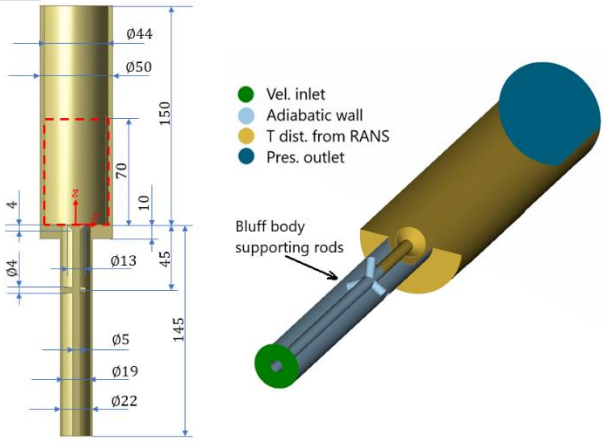

FIGURE 1. MEASUREMENTS (IN MM) OF BURNER CAD GEOMETRY AND BOUNDARY CONDITIONS OF COMPUTATIONAL DOMAIN (DASHED WINDOW REFERS TO THE X-Z COMPARISON PLANE).

Dynamic kinetic energy SGS model is selected, which solves an equation for k_{SGS}. The default wall boundary treatment in Fluent was used [24], which applies laminar stress-strain relation when the mesh is fine enough to resolve the laminar sublayer, and applies the law of the wall otherwise. The SIMPLE scheme with second order implicit transient formulation is

selected for time discretization. For spatial discretization, second order discretization is used for pressure, bounded central differencing is used for momentum, and the QUICK scheme was selected for the remaining scalar transport equations.

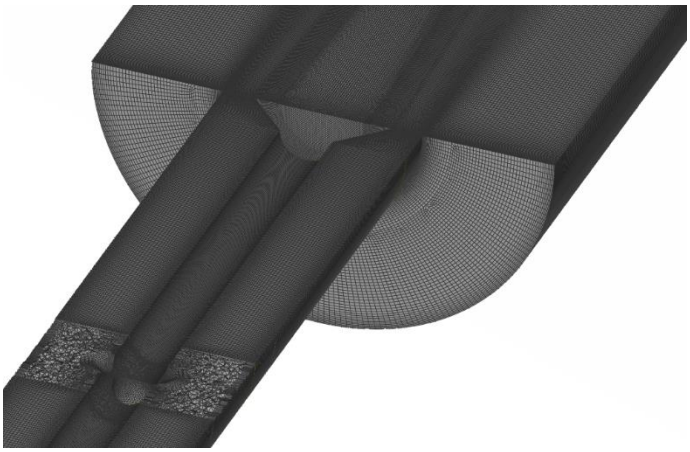

FIGURE 2. COMPUTATIONAL GRID SECTION VIEW.

Calculations and experiments have been performed at atmospheric pressure. The thermal conductivities and viscosities of the mixture were calculated across the flame in Cantera for all fuel blends and were introduced as temperature dependent polynomial coefficients in the CFD solver. The thermal wall boundary conditions are introduced as temperature distributions at walls as indicated in Figure 1. These distributions are obtained from the previous RANS calculations [9] where the conjugated heat transfer was solved for the same cases. The LES cases are initialized from these RANS solutions.

Combustion models are defined via UDFs (User Defined Function). After initialization, statistically steady condition is obtained after 10 flow-through-times. Mean properties are plotted averaging over 2 flow-through-times after steadiness is achieved. Averaging over 4 flow-through-times was also tried and no difference on mean flame shape and mean axial heat release rate (HRR) was observed.

4. RESULTS AND DISCUSSION

The mesh resolution is tested with the Çelik LES quality indicator [25]:

$$IQ_{LES,\nu} = \frac{1}{1 + 0.05\left[\frac{\nu + \nu_{SGS}}{\nu}\right]^{0.53}} \qquad (17)$$

Figure 3 shows $IQ_{LES,\nu}$ values at various section planes in the computational domain for the cold flow and reacting flow cases corresponding to the 0% H_2 case in Table 1. For a good quality LES simulation, resolving minimum 80% of kinetic energy, $0.8 \leq IQ_{LES,\nu} \leq 1$ is suggested in [25]. As observed from Figure 3, the mean value of $IQ_{LES,\nu}$ is varying between 0.9 to 0.95 for the cold flow and varies in a higher range for reacting flow, which confirms the sufficient resolution of the LES mesh, used in this study.

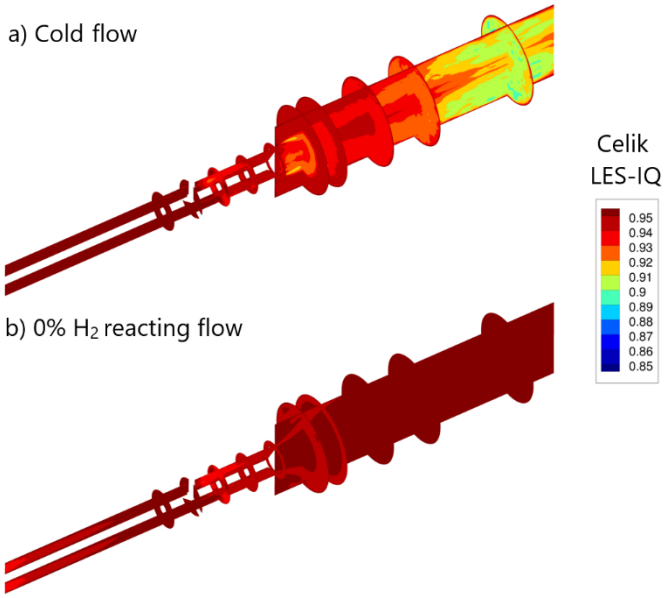

FIGURE 3. MEAN $IQ_{LES,\nu}$ CONTOURS, A) COLD FLOW, B) 0% H_2 REACTING FLOW.

4.1 Cold flow results

For the cold flow conditions of case 1 in Table 1, Figure 4 shows the velocity power spectral density (PSD) measured by a hot-wire and sampled from LES at a point in the middle of the inlet pipe at the dump plane.

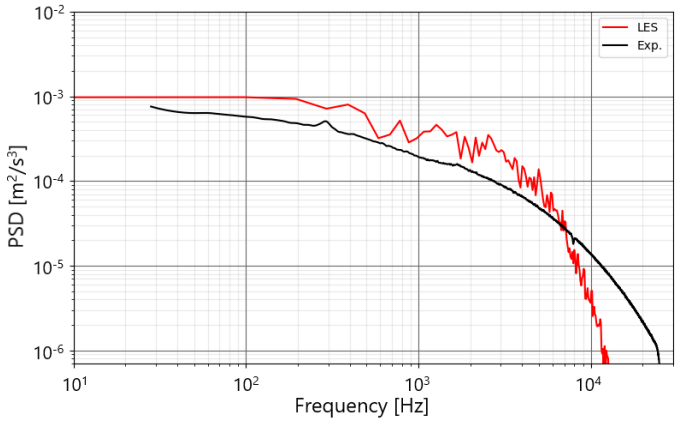

FIGURE 4. PSD COMPARISON OF SAMPLED VELOCITY SIGNALS FROM COLD FLOW EXPERIMENT AND LES AT A POINT ($x = -8\ mm, y = 0\ mm, z = 0\ mm$).

A relatively good agreement between the experiment and the LES is achieved. Calculated and measured PSD curves have the same slope up to high frequency range (around 10^4 Hz) showing that LES could capture the correct characteristics of the flow for

the large scales of turbulence. Deviation of the slope around 10^4 Hz (small scales of turbulence) is attributed to the SGS model used in the LES.

In Figure 5, mean and RMS (root mean square) values of the axial and transversal velocities for the case with $u_{inlet} = 11.8\ m/s$ (the representative for the cases with 0-67% H_2) from cold flow experiment are compared with the cold flow LES. The asymmetric axial velocity distribution due to supporting rods is captured well by LES in the mean velocity plots with some small deviations in the RMS plots. LES slightly over-predicts the axial velocity RMS for positive x values while providing very good agreement for negative x values. Similar trends are also observed in transversal velocity plots, having good agreements in the mean velocity plots. In the RMS plots LES slightly over-predicts the experimental values.

4.2 Reacting flow results without acoustic forcing

LES of the unforced reacting flows were carried out for all the fuel mixtures in Table 1. Figure 6 shows on the left the normalized heat release rate (HRR) contours at the middle cross plane (X-Z comparison plane shown in Figure 1) and the axial HRR distributions from LES simulations in comparison with the Abel deconvoluted OH^* chemiluminescence images and axial intensity plots from experiments. Normalization of axial HRR distributions from LES is done provided that the area under the distribution from experiments (based on OH^* chemiluminescence) and the LES is the same. This represents that the total heat release from LES is equal to those from experiments.

In Figure 6 d, vertical dashed lines show the flame centroid heights $h_{cent.}$, calculated as:

$$h_{cent.} = \frac{\int z\bar{q}\, dz}{\int \bar{q}\, dz} \qquad (18)$$

where z is the axial coordinate, $\bar{q}$ is the heat release rate integrated over planes normal to the z axis. $h_{cent.}$ is plotted separately in Figure 7 for different mixtures.

As observed from Figure 6 a, b and c, both models could capture the correct flame stabilizations for all the cases, i.e. the V-flame to the M-flame shape transition. This is achieved due to the inclusion of stretch and heat loss effects in the formulations through Eq. (10). The importance of such effects on the correct stabilization of the flames was shown in previous studies [1, 7, 9, 22, 23].

Comparing Figure 6 a and c for the mixtures, the ExtH_2TFC model over-predicts the flame length for the case with 0% H_2, while under-predicts it for the other mixtures. On the other hand, the ExtH_2LV model predicts correct flame lengths for all the mixtures (see Figure 6 b and c for the mixtures) except for the 0% H_2 case where it is under-predicted.

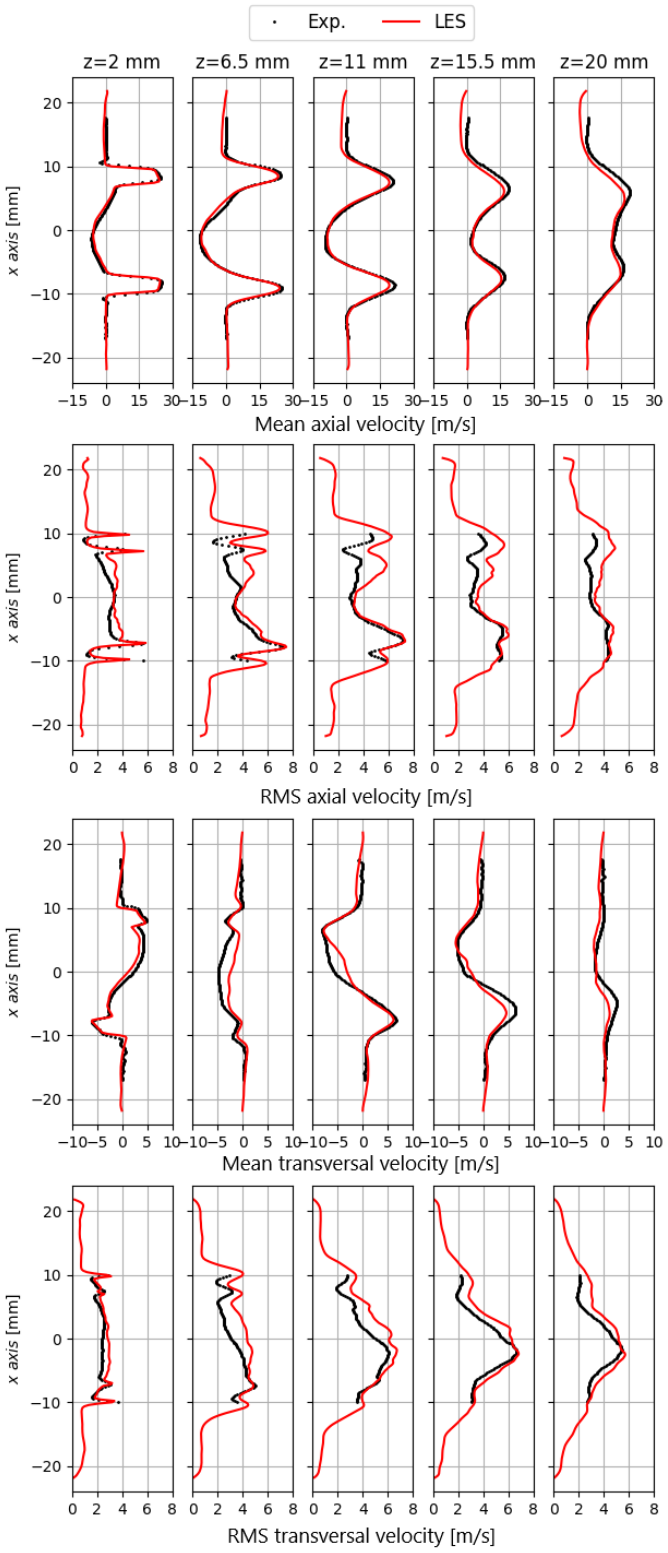

FIGURE 5. EXPERIMENT VS LES COMPARISON PLOTS OF AXIAL AND TRANSVERSAL MEAN AND RMS VELOCITIES FROM COLD FLOW.

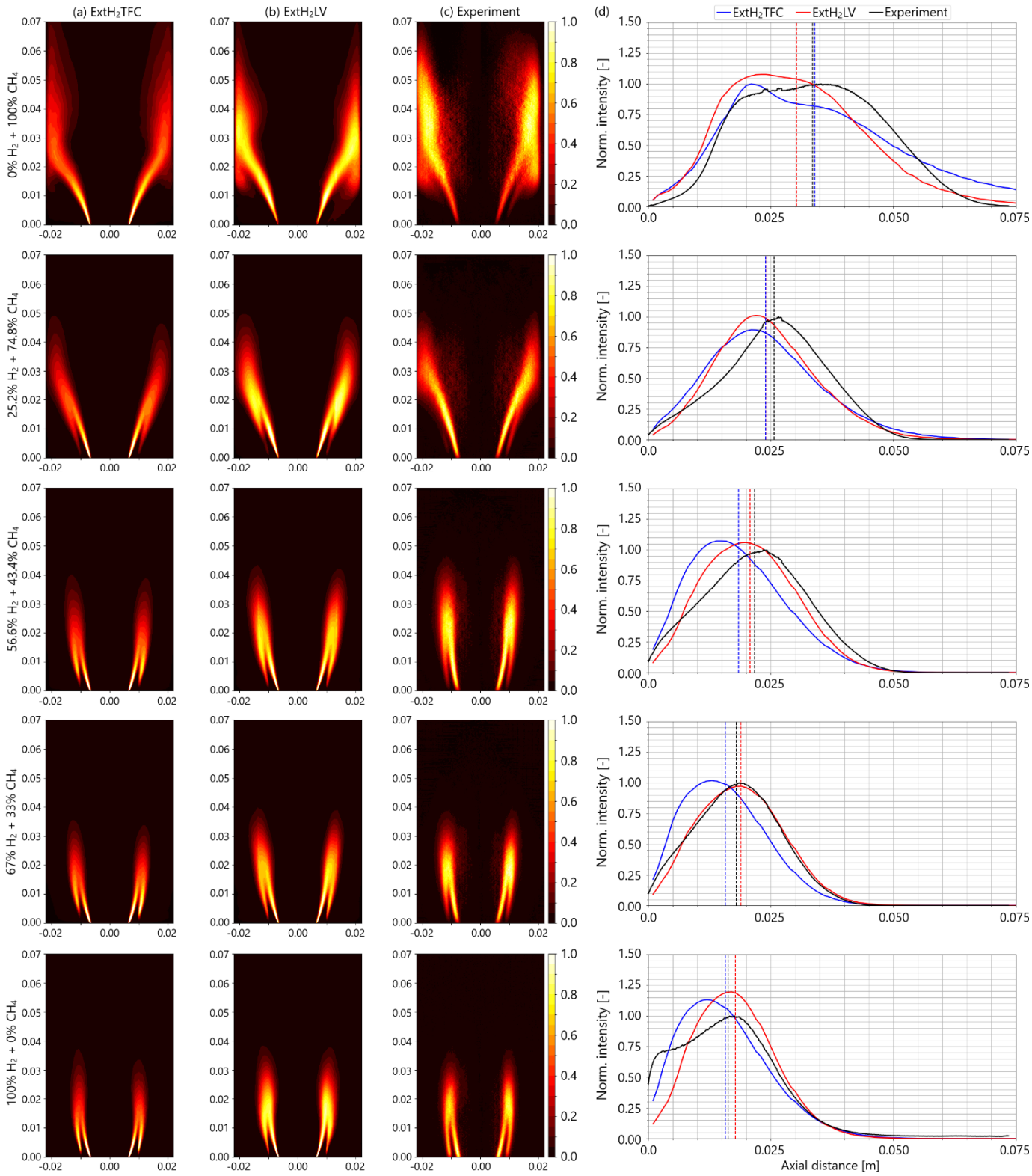

FIGURE 6. HEAT RELEASE RATE DISTRIBUTIONS FROM 2 DIFFERENT LES MODELLING APPROACHES: A) ExtH$_2$TFC, B) ExtH$_2$LV, AND C) ABEL DECONVOLUTED OH* CHEMILUMINESCENCE IMAGES FROM EXPERIMENTS. D) NORMALIZED AXIAL HEAT RELEASE DISTRIBUTIONS ARE SHOWN IN THE RIGHT COLUMN. CONTOUR VALUES ARE NORMALIZED WITH THE MAXIMUM LOCAL INTENSITY. DASHED LINES REFER TO FLAME CENTROID HEIGHTS CALCULATED FROM EQ. (18). CONTOURS ARE PLOTTED AT THE X-Z COMPARISON PLANE SHOWN IN FIGURE 1 WITH RED DASHED RECTANGLE.

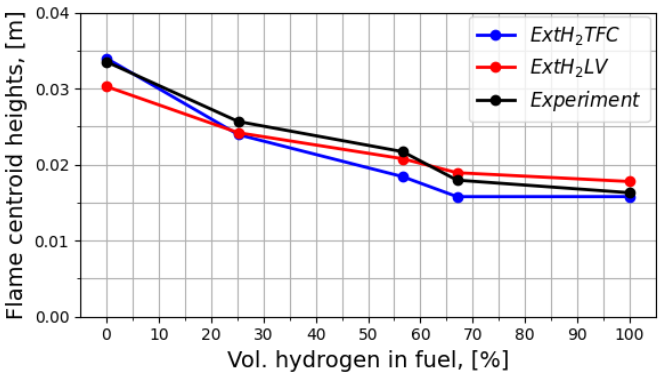

FIGURE 7. FLAME CENTROID HEIGHT VARIATION AGAINST VOLUMETRIC H_2 CONTENT IN THE FUEL MIXTURE.

Figure 6 d shows that the HRR distributions are better predicted with ExtH$_2$LV model compared to ExtH$_2$TFC, as the peaks of the ExtH$_2$TFC model curves are biased towards the dump plane ($z = 0\,mm$ plane). ExtH$_2$LV model curves show more uniform distributions similar to experimental ones. This is also observed from contour plots, comparing Figure 6 a and b, HRR contours intensify towards the dump plane (max HRR is reached at the dump plane) in the ExtH$_2$TFC model, while ExtH$_2$LV model contours exhibit more uniform distributions which are also seen in the experiments. The main reason is that ExtH$_2$TFC model is proportional to the gradient of progress variable $\bar{\dot{\omega}} \propto |\nabla \tilde{c}|$ which takes its maximum value at the flame attaching points to the solid zones. On the other hand, ExtH$_2$LV model also takes its maximum value at the flame attaching points due to its dependency on turbulent dissipation rate through $\bar{\dot{\omega}} \propto \frac{\varepsilon}{k} \approx \frac{\sqrt{k_{sgs}}}{\Delta_{LES}}$. However, the variation of this term from walls to the flow field is not strong as the gradient term $|\nabla \tilde{c}|$, and secondly the variation of $\frac{\varepsilon}{k} \approx \frac{\sqrt{k_{sgs}}}{\Delta_{LES}}$ term is further smoothed by the multiplication with the $\tilde{c}(1-\tilde{c})$ term in the ExtH$_2$LV closure.

For the cases with 100% H_2, both models over-predict the outer shear layer quenching (see the last row of Figure 6 a, b and c). This causes discrepancies in the axial HRR distribution plots (see Figure 6 d) in the region close to the dump plane ($z = 0\,mm$). This over-quenching at the outer shear layer for the case with 100% H_2 was also observed in the previous RANS calculations [1, 9]. To elaborate this behavior, heat loss parameter β, total stretch κ, and interpolated consumption speed S_c contours over the domain are plotted in Figure 8 together with the tabulated laminar consumption speed. The over-quenched region for the case with 100% H_2 is indicated with black circles in the heat loss, stretch and consumption speed contour plots in Figure 8 a, b and c. The corresponding region in the consumption speed tabulation plot is also indicated with a black rectangle in Figure 8 d. As it can be observed, calculated stretch and beta heat loss parameter values correspond to the region where the steep gradients occur in the tabulated S_c curves, and causes abrupt extinctions.

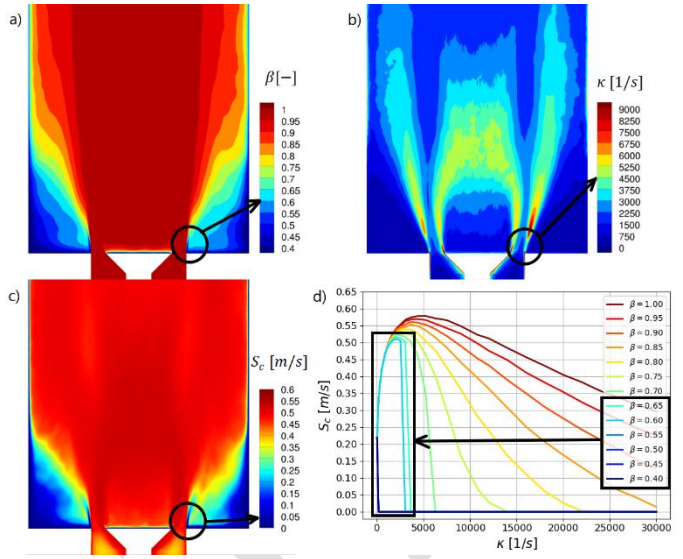

FIGURE 8. X-Z COMPARISON PLANE A) MEAN β, HEAT LOSS PARAMETER CONTOURS, B) MEAN κ, TOTAL STRETCH CONTOURS, C) MEAN S_c, INTERPOLATED CONSUMPTION SPEED CONTOURS AND D) S_c, TABULATED LAMINAR CONSUMPTION SPEED PLOT, OF 100% H_2 + 0% CH_4 FLAME (FROM ExtH$_2$LV LES SIMULATION).

Comparing the flame centroid heights in Figure 7, despite small deviations, both models could correctly capture the center of HRR distributions for all the mixtures which is important in terms of time delay predictions under acoustically forced conditions.

Figures 6 and 7 show that, ExtH$_2$LV model predicts the flame stabilizations in very good agreement with experiments in terms of flame shape, axial HRR distribution and of flame length. With slight deviations in terms of HRR distribution over the flame, ExtH$_2$TFC also predicts the flame stabilizations in good agreement with experiments. However, due to better performance of the ExtH$_2$LV model, it was chosen for the flame dynamics studies. The comparison of flame dynamics with the ExtH$_2$TFC model is subject of future studies.

4.3 Flame dynamics

The flame transfer function (FTF) represents the dynamic response of the flame to acoustic perturbations. Its gain (magnitude) indicates the intensity of heat release rate fluctuations and its phase (angle) provides information about the time delay. Both are influenced by the length of the flame. The FTF is defined as the ratio of heat release rate fluctuations to velocity fluctuations in the frequency domain.

$$FTF(\omega) = \frac{Q'(\omega)/\bar{Q}}{\hat{u}'_{ref}(\omega)/\bar{\hat{u}}_{ref}} \tag{19}$$

where ω refers to the angular frequency, Q is the heat release (volume integrated heat release rate) and $\hat{u}_{ref}$ is the instantaneous mass weighted averaged axial velocity at a

reference plane chosen upstream of the flame. The fluctuations (′) are normalized with the mean values (¯).

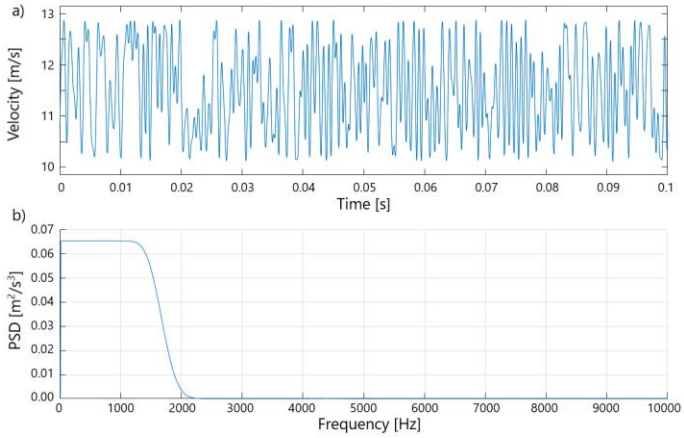

FIGURE 9. A) BROADBAND WAVELET EXCITATION SIGNAL, AND B) POWER SPECTRAL DENSITY PLOTS FOR THE MIXTURE WITH VOLUMETRIC FUEL CONTENT OF 56.6% H_2 + 43.3% CH_4.

The capability of the ExtH_2LV model to capture flame dynamics is investigated based on the extraction of flame transfer functions with LES-SI methods and their comparison to experimental FTFs. For this purpose, TFDtools [26] libraries, developed by Prof. Polifke's research group at TUM (Technical University of Munich) are used for the creation of excitation signals and the extraction of FTFs. The cases are excited with a broadband wavelet signal of 12% of amplitude and the signal length is kept equal to 4 flow-through-times. This corresponds approximately to a signal-to-noise-ratio of 8 in the amplitude of the excitation signal, and to 10 times the longest time delay for the signal length, which guarantees an identification quality of over 90% according to ref. [27]. As an example, the broadband signal and its PSD is shown in Figure 9 for the case with 56.6% H_2. As observed from Figure 9 a, the excitation signal is white noise in nature and its energy is uniformly distributed within the entire frequency band (Figure 9 b). The frequency range is selected to cover the maximum cut-off frequency observed in the experiments.

In Figure 10, the gain and phase of the FTFs are plotted for the different H_2 contents. Comparing the experimental FTFs (dotted lines), the M flames (56.6%, 67% and 100% H_2) show oscillations in the FTF gain, while the V flames (0% and 25.2% H_2) do not. These oscillations were investigated in [3, 28] and it was indicated that, their presence is due to the vortex shedding from the cylindrical supporting rods shown in Figure 1. These vortices perturb the flame as they are travelling into it and cause modulations in the total heat release and consequently in the FTF gain due to convective-acoustic interference. Flames whose cut-off frequency ($\omega_c = 2\pi\hat{u}_{ref}/h_{cent.}$) is higher than the vortex shedding frequency ($\omega_c > \omega_s$, i.e. shorter flames) are prone to show modulations in FTF gain, due to convective interference between shed vortices and acoustic velocity fluctuations which can augment or annihilate flame surface area [3, 28]. Cut-off frequencies are calculated for the cases with 0% and 25.2% H_2 in Appendix B. Vortices do not cause large changes in the total heat release of V flames mainly because these flames are longer (have lower cut-off frequency) compared to M flames and vortices can affect only the inner shear layer (the outer shear layer being quenched). In Figure 11 the different interaction between vortices for M and V flames is shown by means of vorticity and heat release contours. Further discussion of these vortex-flame interaction is provided in [3, 28].

Figure 10 a shows good agreement between ExtH_2LV model and experiment for the V flame case with 0% H_2, in terms of general trends of the gain and phase plots. Shifted gain and over-predicted phase curves in the ExtH_2LV model predictions is the possible result of shorter flame length prediction compared to experiments (see the case with 0% H_2 in Figure 6).

M flame cases with 56.6% and 67% H_2 show excellent agreements in the phase and very good agreements in the gain plots (see Figure 10 c and d). Relating FTF gain and phase with global heat release and flame length, respectively, ExtH_2LV model correctly predicts the flame dynamics for these cases. For these cases, very good agreements were achieved in the mean flame shape, length and axial HRR distribution plots. Additionally, these cases are relatively insensitive to thermal wall boundary conditions due to being stabilized as M flames with some distances from the side walls.

For the case with 100% H_2, similar to the other M flame cases (cases with 56.6% and 67% H_2) excellent agreement is achieved for the FTF phase (see Figure 10 e phase plot). On the other hand, discrepancies are present in the gain plot (see Figure 10 e gain plot). In comparison to the other M flame cases, this case is affected more by the thermal wall boundary condition, and this is observed by the over-quenching at the outer shear layer in the mean flame shape and with disagreement around $z = 0\ mm$ region at axial HRR distribution (see Figure 6) plots. The reason of relatively high sensitivity to heat losses is that, in this case, the equivalence ratio is 0.4 (lower flame temperature) while it is 0.7 for all the other cases (see Table 1). Consequently, thermal boundary conditions used for this case may have caused relatively higher heat losses than reality, resulting in over-quenching at the outer shear layer (see Figure 8) and accordingly discrepancies in the FTF gain plots.

Comparing FTF gains from ExtH_2LV model and experiment for the case with 25.2% H_2, results show that modulations are present in the model prediction, while they are not in experiments (see Figure 10 b, gain plot). On the other hand, reasonably good agreement is achieved for the phase plot (see Figure 10 b, phase plot). This case can be assumed as a transitional operation point between V to M flame (see Figure 6) which makes the most sensitive case to both heat losses and flow disturbances. Figure 6 shows that ExtH_2LV model prediction for the mean flame shape and axial distribution is in good agreement with experiment but with a slight under-prediction in flame length. This is also seen from flame centroid heights comparison in Figure 7. Possible explanation for the disagreement in gain plot in Figure 10 b is that, although the mean flame is predicted

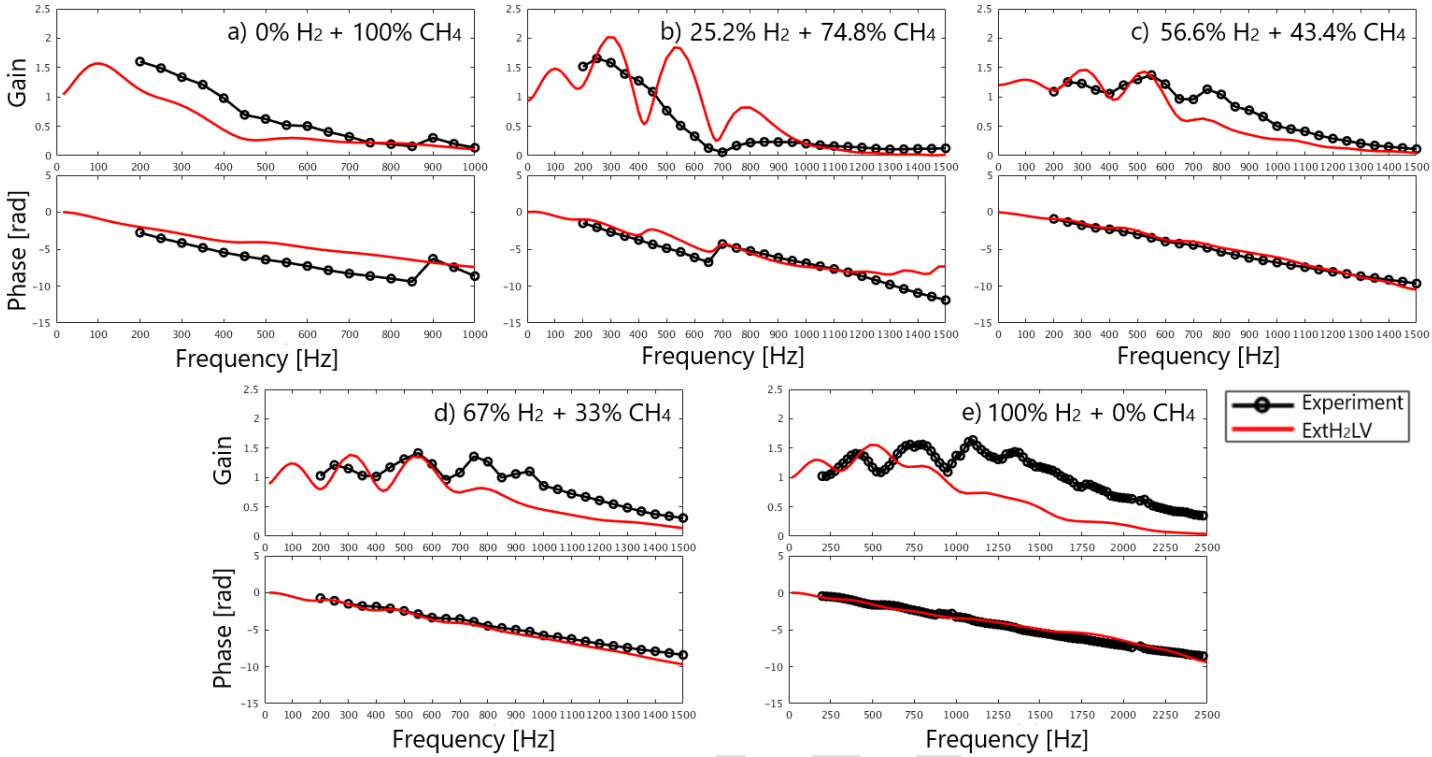

FIGURE 10. FLAME TRANSFER FUNCTION COMPARISON PLOTS (EXPERIMENT VS ExtH$_2$LV LES MODEL).

as V flame, due to its shorter length compared to experiment, the ExtH$_2$LV model flame has higher cut-off frequency than the vortex shedding frequency ($\omega_c > \omega_s$), which provides suitable condition (see Appendix B) for modulations as mentioned above and remarked in [3].

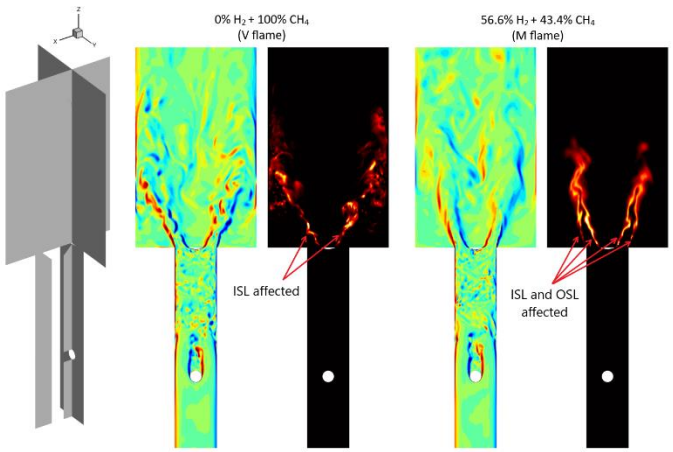

FIGURE 11. INSTANTANEOUS X VORTICITY AND HEAT RELEASE RATE CONTOURS PLOTTED ON Y-Z PLANE (FROM ExtH$_2$LV LES SIMULATION).

It is noteworthy to mention that wall temperature measurements were not performed in the experiments, instead there were rough measurements from a similar setup (square sectioned combustion chamber operated with an ethylene flame). For these measurements, the temperature was in the range of 593 K – 833 K (at different locations from z = 0.01 m to z = 0.03 m) on the outside surface of the combustor wall. Using these rough measurements, a parametric RANS study was conducted (not in this paper) to find a proper heat transfer coefficient (HTC) at side walls by assigning different HTCs. HTC = 150 W/m^{2}K produced reasonable agreement on wall temperatures and flame shapes in the RANS context, and that value kept as constant for all the cases [1, 9]. Obtained temperature distributions from RANS cases were assigned as temperature distributions at walls in this study.

For the cases with 0% and 25.2% H$_2$, to test the model's sensitivity to heat losses, different levels of heat losses were simulated changing the side wall HTC in the LES context (not presented in this paper for brevity). It was seen that varying HTC on the side walls in a range from 100 to 200 W/m^{2}K produced very similar flame lengths. On the other hand, the model coefficient A, together with the Le^* number has a direct impact on the heat release rate and the flame length ($\bar{\omega} \propto \frac{A}{\sqrt{Le^*}}$) [1]. The model coefficient A for the ExtH$_2$LV was calibrated based on turbulent flame speed measurements and validated using this configuration. Further investigations in other configurations will be carried out to confirm the transferability of this value to other conditions and geometries. As a further extension, the Le^* number can be considered as a field variable depending also on stretch and heat losses rather than on mixture fraction only as calculated in this study.

The ExtH$_2$LV model is capable to predict the general trends of FTF gain and phase plots in good agreement with experiments. The impact of the supporting rods on the flame dynamics seen in experiments of the M-flame cases are also captured by the model. The detailed analysis of the rods on the flame dynamics using CFD is part of future studies.

5. CONCLUSION

A novel premixed combustion model (ExtH$_2$LV) is proposed for turbulent CH$_4$/H$_2$/air flames. The model accounts for flame stretch, heat losses and effective Lewis number in LES context. Stretch, heat loss and Lewis number effects are introduced by means of a previously proposed turbulent flame speed expression. The model is validated with atmospheric bluff-body stabilized CH$_4$/H$_2$/air turbulent premixed flame experiments ranging from pure methane to pure hydrogen under lean mixture conditions. The ExtH$_2$LV model is compared with the authors' previously proposed model (ExtH$_2$TFC) and experiments. Both models are derived for the RANS closure and then transformed into LES models using proper relations. The ExtH$_2$LV model does not need model coefficient re-adjustment for its transformation to LES context.

In the proposed ExtH$_2$LV closure as well as in the ExtH$_2$TFC closure, stretch and heat loss modelling approaches (Eq. 14, 15 and 16) are responsible for the mean flame shape and stabilization, while the model coefficient A, together with Le^* is responsible for the flame length ($\bar{\dot{\omega}} \propto \frac{A}{\sqrt{Le^*}}$). Thanks to the inclusion of stretch, heat loss and Lewis number effects in their formulations, both models could correctly predict the flame stabilizations and the V to M flame transition as H$_2$ content in the mixture increases. ExtH$_2$LV showed improvements with respect to ExtH$_2$TFC in the mean flame shapes.

The ExtH$_2$LV model is also tested for its capability to reproduce flame dynamics under acoustically forced conditions via identification of FTFs which are compared against experiments. Results show that the ExtH$_2$LV model is capable of reproducing flame dynamics with good agreement with experiments. It is also shown that the correct flame stabilization in the mean flame shape does not guarantee the correct flame dynamics. Heat loss effects and hydrodynamic disturbances on flame dynamics are discussed and it is shown that their effects can become prominent under certain conditions.

To place the proposed ExtH$_2$LV modelling approach amongst the others in the literature, the pros and cons can be listed as follows. For its pros: it can be used for premixed flame simulations in RANS and LES context with detailed chemistry approach. Stretch, heat loss and Lewis number effects can simply be accounted for through algebraic relations of turbulent flame speed S_t and reaction rate $\bar{\dot{\omega}} \propto S_t$ terms. The validity range of the modelling approach for high pressure and partially premixed conditions can be extended through further calibrations of the turbulent flame speed against spherical expanding turbulent flame measurements as explained in [1]. For its cons: since the reaction rate term is function of turbulence parameters ($\bar{\dot{\omega}} \propto \frac{\varepsilon}{k} \approx \frac{\sqrt{k_{sgs}}}{\Delta_{LES}}$), due to increased turbulent dissipation rate and decreased kinetic energy, the model over-predicts reaction rates where the flame interacts with the walls. To remedy this phenomenon, further studies on wall quenching models can be incorporated in the modelling approach.

As future steps, investigation on the model predictions with more accurate thermal wall boundary conditions, and extension of the model validation range to high pressure, rich and/or partially premixed conditions, where diffusivity effects are more important, are planned.

ACKNOWLEDGEMENTS

The authors are thankful to Prof. Wolfgang Polifke from Technical University of Munich, Germany, for making available TFDtools used for the system identification purposes in this study. The supports from Edoardo Scoletta for the usage of the TFDtools, and fruitful discussions with him and Prof. Polifke are acknowledged.

This work is part of the Marie Skłodowska-Curie Initial Training Network Pollution Know-How and Abatement (POLKA). The authors gratefully acknowledge the financial support from the European Commission under call H2020-MSCA-ITN-2018 (project number: 813367).

APPENDIX A: ExtH$_2$LV MODEL DERIVATION

The flame surface density Σ can be modelled from fractal theories as in [14, 29].

$$\Sigma = \left(\frac{L_o}{L_i}\right)^{D-2} \frac{\tilde{c}(1-\tilde{c})}{\delta_t} \tag{A.1}$$

In Eq. (A.1), L_i and L_o represent the inner and outer cut-off scales, respectively, D is the fractal dimension of the flame surface ($2 \leq D < 3$) and δ_t is the turbulent flame brush thickness [29]. The $\tilde{c}(1-\tilde{c})$ term represents the probability of finding the flame at a certain position and δ_t is used to normalize the probability value [29]. L_i and L_o can be modelled using the Kolmogorov and turbulent integral length scales as:

$$L_i = \eta_K = \frac{\nu^{0.75}}{\varepsilon^{0.25}}, \quad L_o = l_t = C_\mu^{0.75} \frac{k^{1.5}}{\varepsilon} \tag{A.2}$$

To model the turbulent flame brush thickness δ_t, it is assumed that δ_t is proportional to the flame surface wrinkling length scale L_y in the BML (Bray-Moss-Libby) model [30]:

$$L_y = C_L l_t \frac{S_{L0}}{u'} \propto \delta_t = \frac{1}{C_\mu^{0.5}} l_t \frac{S_{L0}}{S_t} \tag{A.3}$$

Comparing L_y and δ_t in Eq. (A.3), turbulent velocity u' is replaced by turbulent flame speed S_t in order to address the stretch, heat loss and Lewis number effects. This change is reasonable, since the relation $S_t \propto (u')^{0.7-0.8}$ is known from the literature studies [1, 31] and $S_t \propto u'$ relation is known from the Damkohler's hypothesis [32].

Additionally, C_L coefficient in L_y in Eq. (A.3) is replaced by $1/C_\mu^{0.5}$ ($C_\mu = 0.09$ as in Eq. (A.2)), as it cancels out when Eq. (A.2) and (A.3) are substituted into Eq. (A.1).

Substituting L_i, L_o and δ_t from Eq. (A.2) and Eq. (A.3) into Eq. (A.1), and assuming $D = 7/3$ as in [14], yields the following expressions for the flame surface density Σ and for the reaction rate source term $\bar{\dot{\omega}}$ in RANS context:

$$\Sigma = \frac{\varepsilon}{k}\frac{S_t}{S_{L0}}\frac{\tilde{c}(1-\tilde{c})}{u_{\eta_K}}, \quad \bar{\dot{\omega}} = \rho_u \frac{S_t}{u_{\eta_K}}\frac{\varepsilon}{k}\tilde{c}(1-\tilde{c}) \qquad \text{(A.4)}$$

where $u_{\eta_K} = (\nu\varepsilon)^{0.25}$ is Kolmogorov velocity scale, k and ε are turbulent kinetic energy and dissipation rate respectively.

APPENDIX B: CUT-OFF FREQUENCIES FOR ExtH$_2$LV LES CASES WITH 0% AND 25.2% H$_2$

The flame response angular cut-off frequency is calculated from Eq. (B.1) following [3]:

$$\omega_c = \frac{2\pi\hat{u}_{ref}}{h_{cent.}} \qquad \text{(B.1)}$$

where $h_{cent.}$ is the flame centroid height, defined by Eq. (18), and $\hat{u}_{ref}$ is the averaged axial velocity at dump plane ($z = 0$). $\hat{u}_{ref}$ and $h_{cent.}$ are obtained from the unforced ExtH$_2$LV LES results for the cases with 0% and 25.2% H$_2$, and the cut-off frequencies are found as $\omega_c = 4354\, rad/s$ and $\omega_c = 5430\, rad/s$, respectively.

The condition for the presence of modulations in FTF gain was given as $\omega_c > \omega_s$ in [3]. Vortex shedding frequency of supporting rods is calculated as $f_s \cong 850\, Hz$, by taking DFT (Discrete Fourier Transform) of the sampled velocity signal at the axial location downstream of the supporting rods (in wake region) from the unforced LES simulation. The angular vortex shedding frequency is calculated as follows.

$$\omega_s = 2\pi f_s = 5340\, rad/s \qquad \text{(B.2)}$$

ω_s (Eq. (B.2)) is the same for the cases with 0% and 25.2% H$_2$, since the inlet bulk velocity is the same for these cases (see Table 1).

Comparison shows that, the $\omega_c > \omega_s$ condition is not satisfied for the case with 0% H$_2$, while is satisfied for the case with 25.2% H$_2$.

REFERENCES

[1] Kutkan, H., Amato, A., Campa, G., Ghirardo, G., Tay-Wo-Chong, L., and Æsøy, E., "Modeling of turbulent premixed CH_4/H_2/air flames including the influence of stretch and heat losses," *Journal of Engineering for Gas Turbines and Power*, vol. 144, no. 1, p. 011020, Jan. 2022. doi: 10.1115/1.4051989.

[2] Æsøy, E., Aguilar, J. G., Wiseman, S., Bothien, M. R., Worth, N. A., and Dawson, J. R., "Scaling and prediction of transfer functions in lean premixed H_2/CH_4-flames," *Combustion and Flame*, vol. 215, pp. 269–282, May 2020. doi: 10.1016/j.combustflame.2020.01.045.

[3] Æsøy, E. Aguilar, J. G., Bothien, M. R., Worth, N. A. and Dawson, J. R., "Acoustic-convective interference in transfer functions of methane/hydrogen and pure hydrogen flames," *Journal of Engineering for Gas Turbines and Power*, vol. 143, no. 12, p. 121017, Dec. 2021. doi: 10.1115/1.4051960.

[4] Guiberti, T. F., Durox, D., Scouflaire, P., and Schuller, T., "Impact of heat loss and hydrogen enrichment on the shape of confined swirling flames," *Proceedings of the Combustion Institute*, vol. 35, no. 2, pp. 1385–1392, 2015. doi: 10.1016/j.proci.2014.06.016.

[5] Mercier, R., Guiberti, T. F., Chatelier, A., Durox, D., Gicquel, O., Darabiha, N., Schuller, T. and Fiorina, B., "Experimental and numerical investigation of the influence of thermal boundary conditions on premixed swirling flame stabilization," *Combustion and Flame*, vol. 171, pp. 42–58, Sep. 2016. doi: 10.1016/j.combustflame.2016.05.006.

[6] Chatelier, A., Guiberti, T. F., Mercier, R., Bertier, N., Fiorina, B. and Schuller, T., "Experimental and numerical investigation of the response of a swirled flame to flow modulations in a non-adiabatic combustor," *Flow Turbulence Combust*, vol. 102, no. 4, pp. 995–1023, Apr. 2019. doi: 10.1007/s10494-018-9995-2.

[7] Tay-Wo-Chong, L., Scarpato, A., and Polifke, W., "LES combustion model with stretch and heat loss effects for prediction of premix flame characteristics and dynamics," in *Proceedings of ASME Turbo Expo 2017*, 2017, pp. 1–12. doi: 10.1115/GT2017-63357.

[8] Nassini, P. C., Pampaloni, D., Meloni, R., and Andreini, A., "Lean blow-out prediction in an industrial gas turbine combustor through a LES-based CFD analysis," *Combustion and Flame*, vol. 229, p. 111391, Jul. 2021. doi: 10.1016/j.combustflame.2021.02.037.

[9] Kutkan, H., Amato, A., Campa, G., Tay-Wo-Chong, L., and Æsøy, E., "Assessment of turbulent premixed combustion models for CH_4/H_2/air flames," in *Proceedings of the 27th International Congress on Sound and Vibration*, 2021, p. 8.

[10] Poinsot, T., and Veynante, D., *Theoretical and Numerical Combustion*, 3rd edition. Bordeaux, France, 2012.

[11] Veynante, D., and Vervisch, L., "Turbulent combustion modeling," *Progress in Energy and Combustion Science*, vol. 28, no. 3, pp. 193–266, Mar. 2002. doi: 10.1016/S0360-1285(01)00017-X.

[12] Boger, M., Veynante, D., Boughanem, H., and Trouvé, A., "Direct numerical simulation analysis of flame surface density concept for large eddy simulation of turbulent premixed combustion," *Symposium (International) on Combustion*, vol. 27, no. 1, pp. 917–925, Jan. 1998. doi: 10.1016/S0082-0784(98)80489-X.

[13] Vervisch, L., and Veynante, D., "Interlinks between approaches for modeling turbulent flames," *Proceedings of the Combustion Institute*, vol. 28, no. 1, pp. 175–183, Jan. 2000. doi: 10.1016/S0082-0784(00)80209-X.

[14] Lindstedt, R., and Vaos, E., "Modeling of premixed turbulent flames with second moment methods," *Combustion and Flame*, vol. 116, no. 4, pp. 461–485, Mar. 1999. doi: 10.1016/S0010-2180(98)00058-3.

[15] Dinkelacker, F., Manickam, B., and Muppala, S. P. R., "Modelling and simulation of lean premixed turbulent methane/hydrogen/air flames with an effective Lewis number approach," *Combustion and Flame*, vol. 158, no. 9, pp. 1742–1749, 2011. doi: 10.1016/j.combustflame.2010.12.003.

[16] Zimont, V. L., and Battaglia, V., "Joint RANS/LES approach to premixed flame modelling in the context of the TFC combustion model," *Flow Turbulence Combust*, vol. 77, no. 1–4, pp. 305–331, Oct. 2006. doi: 10.1007/s10494-006-9048-0.

[17] Allauddin, U., Lomada, S. R. R., and Pfitzner, M., "Investigation of pressure and the Lewis number effects in the context of algebraic flame surface density closure for LES of premixed turbulent combustion," *Theor. Comput. Fluid Dyn.*, vol. 35, no. 1, pp. 17–37, Feb. 2021. doi: 10.1007/s00162-020-00543-x.

[18] Manickam, B., Franke, J., Muppala, S. P. R., and Dinkelacker, F., "Large-eddy Simulation of triangular-stabilized lean premixed turbulent flames: Quality and error assessment," *Flow Turbulence Combust*, vol. 88, no. 4, pp. 563–596, Jun. 2012. doi: 10.1007/s10494-011-9385-5.

[19] Goodwin, D. G., Speth, R. L., Moffat, H. K., and Weber, B. W., *Cantera 2.4.0*. 2018. [Online]. Available: https://www.cantera.org.

[20] Metcalfe, W. K., Burke, S. M., Ahmed, S. S., and Curran, H. J., "A hierarchical and comparative kinetic modeling study of C_1-C_2 hydrocarbon and oxygenated fuels: Kinetic study of C_1-C_2 hydrocarbon and oxygenated fuels," *Int. J. Chem. Kinet.*, vol. 45, no. 10, pp. 638–675, Oct. 2013. doi: 10.1002/kin.20802.

[21] Bougrine, S., Richard, S., Colin, O., and Veynante, D., "Fuel composition effects on flame stretch in turbulent premixed combustion: Numerical analysis of flame-vortex interaction and formulation of a new efficiency function," *Flow Turbulence Combust*, vol. 93, no. 2, pp. 259–281, Sep. 2014. doi: 10.1007/s10494-014-9546-4.

[22] Tay-Wo-Chong, L., Komarek, T., Zellhuber, M., Lenz, J., Hirsch, C., and Polifke, W., "Influence of strain and heat loss on flame stabilization in a non-adiabatic combustor," in *European Combustion Meeting*, 2009, no. May 2014, pp. 1–6.

[23] Tay-Wo-Chong, L., Zellhuber, M., Komarek, T., Im, H. G. and Polifke, W., "Combined influence of strain and heat loss on turbulent premixed flame stabilization," *Flow, Turbulence and Combustion*, vol. 97, no. 1, pp. 263–294, 2016. doi: 10.1007/s10494-015-9679-0.

[24] Ansys Fluent v19.3, *Fluent Theory Guide*. 2019.

[25] Celik, I. B., Cehreli, Z. N. and Yavuz, I., "Index of resolution quality for large eddy simulations," *Journal of Fluids Engineering*, vol. 127, no. 5, pp. 949–958, Sep. 2005. doi: 10.1115/1.1990201.

[26] Polifke, W., *TFDtools*. private communication 2021.

[27] Huber, A., and Polifke, W., "Dynamics of practical premixed flames, part I: Model structure and identification," *International Journal of Spray and Combustion Dynamics*, vol. 1, no. 2, pp. 199–228, Jun. 2009. doi: 10.1260/175682709788707431.

[28] Æsøy, E., Nygård, H. T., Worth, N. A., and Dawson, J. R., "Tailoring the gain and phase of the flame transfer function through targeted convective-acoustic interference," *Combustion and Flame*, vol. 236, p. 111813, Feb. 2022. doi: 10.1016/j.combustflame.2021.111813.

[29] Gouldin, F. C., Bray, K. N. C., and Chen, J. Y., "Chemical closure model for fractal flamelets," *Combustion and Flame*, vol. 77, no. 3–4, pp. 241–259, Sep. 1989. doi: 10.1016/0010-2180(89)90132-6.

[30] Bray, K. N. C., "Studies of the turbulent burning velocity," *Proc. R. Soc. Lond. A*, vol. 431, no. 1882, pp. 315–335, Nov. 1990. doi: 10.1098/rspa.1990.0133.

[31] Zimont, V. L., "Gas premixed combustion at high turbulence. Turbulent flame closure combustion model," *Experimental Thermal and Fluid Science*, p. 8, 2000. doi: 10.1016/S0894-1777(99)00069-2.

[32] Driscoll, J. F., Chen, J. H., Skiba, A. W., Carter, C. D. Hawkes, E. R., and Wang, H., "Premixed flames subjected to extreme turbulence: Some questions and recent answers," *Progress in Energy and Combustion Science*, vol. 76, p. 100802, Jan. 2020. doi: 10.1016/j.pecs.2019.100802.